Composites Part B 186 (2020) 107814

Contents lists available at ScienceDirect

Composites Part B

journal homepage: www.elsevier.com/locate/compositesb

Epoxy resin thermo-mechanics and failure modes: Effects of cure and cross-linker length

Sanjib C. Chowdhury [a,*], Robert M. Elder [e,f], Timothy W. Sirk [e], John W. Gillespie Jr. [a,b,c,d]

[a] Center for Composite Materials (UD-CCM), University of Delaware, Newark, DE, 19716, USA
[b] Department of Materials Science & Engineering, University of Delaware, Newark, DE, 19716, USA
[c] Department of Civil & Environmental Engineering, University of Delaware, Newark, DE, 19716, USA
[d] Department of Mechanical Engineering, University of Delaware, Newark, DE, 19716, USA
[e] Macromolecular Science and Technology Branch, U.S. Army Research Laboratory, Aberdeen, MD, 21005, USA
[f] Bennett Aerospace, Inc., Cary, NC, 27511, USA

ARTICLE INFO

Keywords:
Cross-linked epoxy
Molecular dynamics simulation
Mechanical properties
Glass transition temperature

ABSTRACT

The effects of molecular weight (MW) of cross-linker and degree of cure on the structure and thermo-mechanical properties of the Bisphenol A diglycidyl ether epoxy resin have been studied using MD simulations with reactive force field ReaxFF and non-reactive General AMBER Force Field (GAFF). Cross-linked structures are created from stoichiometric mixtures of Epon and Jeffamine® using a multi-step cross-linking algorithm. The glass transition temperature (T_g) is determined by annealing where the cross-linked epoxy is cooled from the rubbery state to below room temperature. Deformation mechanisms of the cross-linked epoxy including bond breakage are studied under tensile and shear loadings. The effects of cross-linkers of increasing MW (Jeffamine® D-230, Jeffamine® D-400 and Jeffamine® D-600) are studied for highly cured (98.5% degree of cure) systems. MD predicted T_g is in good agreement with experiments after cooling rate correction using the WLF relationship. The highest T_g is obtained for the lower MW cross-linker that exhibits a denser network structure. In addition, the effects of varying degrees of cure on properties are studied for Epoxy/Jeffamine® D-230. In this case, the MD results shows that T_g increases linearly with degree of cure and that the DiBenedetto relationship can be applied using the MD fitted parameters. Lower MW cross-linker yields higher modulus and yield stress and reduced strain to failure and energy absorption than the higher MW cross-linkers. Results from GAFF, which is about 100 times more computationally efficient, agree well with ReaxFF predictions up to the strain limit at which bond breakage becomes significant.

1. Introduction

Epoxy, a thermosetting polymer, is widely used in coatings, adhesives, electronics packaging and high performances composite structural applications. Fiber reinforced epoxy composites are one of the primary structural materials used in lightweight aircraft, helicopters and ground vehicles. In structural composites, the cured epoxy serves as the matrix material that transfers load to the fibers. The glass transition temperature of the epoxy matrix determines the maximum service temperature of the structure. In addition, the mechanical properties, energy absorption and damage tolerance of the composite are very sensitive to the properties of the epoxy matrix as well as the other composite constituents (e.g. fiber and interphase).

Cured or cross-linked epoxies are made from the chemical reactions of two components – epoxy resin and cross-linker (i.e., curing agent or hardener). There are various types of epoxy resins and curing agents. For instance, Bisphenol A diglycidyl ether (Epon 825) epoxy with Jeffamine® curing agents are used as matrix materials in glass and carbon fiber reinforced polymer composites. A wide range of matrix processing characteristics, thermal and mechanical properties can be achieved through the incorporation of various MW Jeffamine® curing agents into the Epon formulations. Optimization of these formulations for specific applications is typically conducted through experimental approaches.

There are some experimental and molecular dynamics (MD) simulation studies that have investigated the effects of the functionality (i.e. di-, tri-, and tetra-) of the curing agents, degree of cure and cross-linker

* Corresponding author.
E-mail address: sanjib@udel.edu (S.C. Chowdhury).

https://doi.org/10.1016/j.compositesb.2020.107814
Received 15 June 2019; Received in revised form 26 August 2019; Accepted 23 January 2020
Available online 27 January 2020
1359-8368/

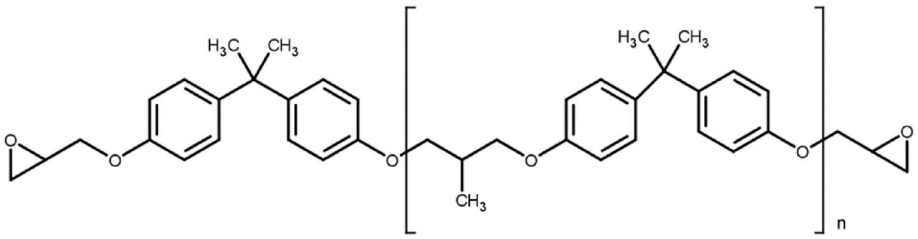

(a) Epon molecule

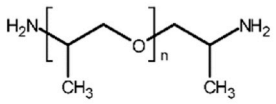

(b) Jeffamine® molecule

Fig. 1. Molecular structure of (a) Epon 825 and (b) Jeffamine®.

length (i.e. molecular weight (MW)) on the structure and thermo-mechanical properties of the epoxy matrix [1–11]. Most of the MD simulation studies have focused on the thermal and tensile elastic properties of epoxy considering non-reactive type force fields which do not have bond breaking and formation capability that prevents energy absorption associated with progressive failure to be predicted. Li et al. [5] have studied the thermo-mechanical properties of Epon 862/DETDA system using the non-reactive DREIDING force field [12]. They found a significant increase in glass transition temperature (T_g), Young's modulus and yield strength with the increase in degree of cure. Varshney et al. [6] have determined the T_g and coefficient of thermal expansion (*CTE*) of the Epon 862/DETDA system using Consistent Valence Force Field (CVFF) [13]. Soni et al. [7] have studied the effects of the cross-linker MW on the DEGBA/Jeffamine® properties using General AMBER Force Field (GAFF) [14,15]. They have reported that T_g decreases and *CTE* increases with increase in the cross-linker length. Sirk et al. [8] have determined T_g and Young's modulus of the DGEBA/-Jeffamine® system using GAFF. Young's moduli are determined at different strain rates across the glass transition temperature and, using time-temperature superposition a master curve for the modulus versus strain rates response has been proposed. Fan et al. [9] have determined the T_g, *CTE* and Young's modulus of Epon 862/TETA system using Polymer Consistent Force Field (PCFF) [16]. Li et al. [17] comprehensively reviewed molecular simulation works based on non-reactive force fields which focus on the structure-properties relationships of thermoset epoxy.

Recently, Odegard et al. [10] have determined the modulus and yield strength of the Epon 832/DETDA epoxy system using reactive force field ReaxFF [18]. Since they were interested in the modulus and yield strength their simulations were limited to lower strain range level (<18% strain) without failure. In another recent MD study with ReaxFF, Meng et al. [19] have predicted macroscopic fracture toughness of cured epoxy by developing a molecularly informed continuum fracture model which considers fibril strength and crazing zone micro-structure.

Though much progress has been made through previous studies, there is still no complete understanding on the structure-properties relationship, energy absorption and failure mechanism of the cured epoxy matrix under tensile loading. None of earlier simulations (except Meng et al. [19]) conducted tensile loading up to failure of the epoxy system to determine the progressive damage modes associated with toughness and energy absorption. There have been no attempts to understand the behavior of the cured epoxy under shear loading at large deformation [20]. However, there are many practical applications where the epoxy based composite materials undergoes large tension-shear deformation and failure. For instance, epoxy resin near a broken fiber in fiber reinforced composites experiences significant deformation under combined tension-shear high strain rate loading [21]. Therefore, it is advantageous to understand the large strain response and failure mechanisms of the epoxy system as a function of cross linker length and degree of cure to design optimal epoxy matrices at the molecular level.

In this paper, the effects of molecular weight of the Jeffamine® cross-linker and degree of cure on the network structure, glass transition temperature, mechanical properties, and deformation and failure

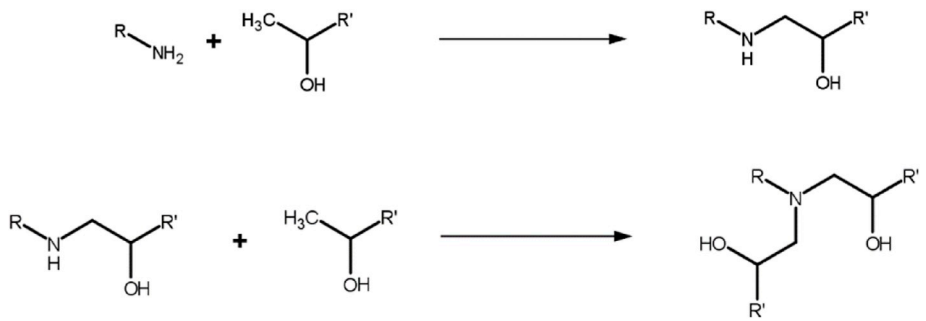

Fig. 2. Curing reaction between epoxide and amine groups of Epon and Jeffamine® molecules.

Table 1a
Molecule data for Epon-Jeffamine® models.

Model Designation	Jeffamine® Molecule	Epon Molecule
Epon/J230	Jeffamine® D-230 (n = 2.6, MW = 225.7 g/mol)	Epon 825 (n = 0.13, MW = 378.8 g/mol)
Epon/J400	Jeffamine® D-400 (n = 6.1, MW = 429.5 g/mol)	
Epon/J600	Jeffamine® D-600 (n = 9.0, MW = 598.4 g/mol)	

Table 1b
Molecule data for Epon-Jeffamine® models.

Model Designation	Number of Epon Molecules	Number of Jeffamine® Molecules	Total atoms
Epon/J230	1740 molecules with n = 0 260 molecules with n = 1	400 molecules with n = 2 600 molecules with n = 3	158180
Epon/J400	1392 molecules with n = 0 208 molecules with n = 1	720 molecules with n = 6 80 molecules with n = 7	154544
Epon/J600	1218 molecules with n = 0 182 molecules with n = 1	700 molecules with n = 9	155526

mechanism of the Epon 825 epoxy resin have been studied using molecular dynamic methods. Large-strain tensile and shear simulations are conducted using reactive force field ReaxFF [18] to determine elastic, yield and strength properties, energy absorption capability and the associated deformation and progressive failure mechanism. The glass transition temperature, which does not require bond breakage, is determined using non-reactive force field GAFF [14,15]. For comparison with ReaxFF prediction, tensile and shear simulations with GAFF are also conducted to identify the limits of applicability of this non-reactive but computationally efficient force field.

2. Molecular simulations details

2.1. Force field

Two types of force fields – non-reactive general Amber force field (GAFF) [14,15] and reactive force field ReaxFF [18,22] are used in the present study. GAFF is used to describe atomic interactions in the cross-linking algorithm, quenching to glassy state, tensile and shear simulations. GAFF is applied for non-reactive simulations due to its good performance in earlier studies of predicting thermodynamics and mechanics for epoxy networks [7,8,11,23,24]. van der Waals interactions are truncated at 0.9 nm with tail corrections applied for the energy and pressure [25]. Partial charges of atoms are calculated using the AM1-BCC method [26,27]. Coulomb interactions are calculated using the particle–particle particle–mesh (PPPM) method with a real-space cut-off of 0.9 nm [28]. Although GAFF provides a good model for many organic molecules, it cannot model bond breaking and formation due in part to the harmonic functional form for the bond interactions.

The state-of-the-art reactive force field ReaxFF is used during the mechanical deformation to capture bond-breaking and formation processes. ReaxFF includes a continuous bond length and bond order relationship and a polarizable, geometry-dependent charge calculation [29,30]. A full description of the ReaxFF potential functions can be found elsewhere [31]. ReaxFF parameters sets developed by Liu et al. [18] are

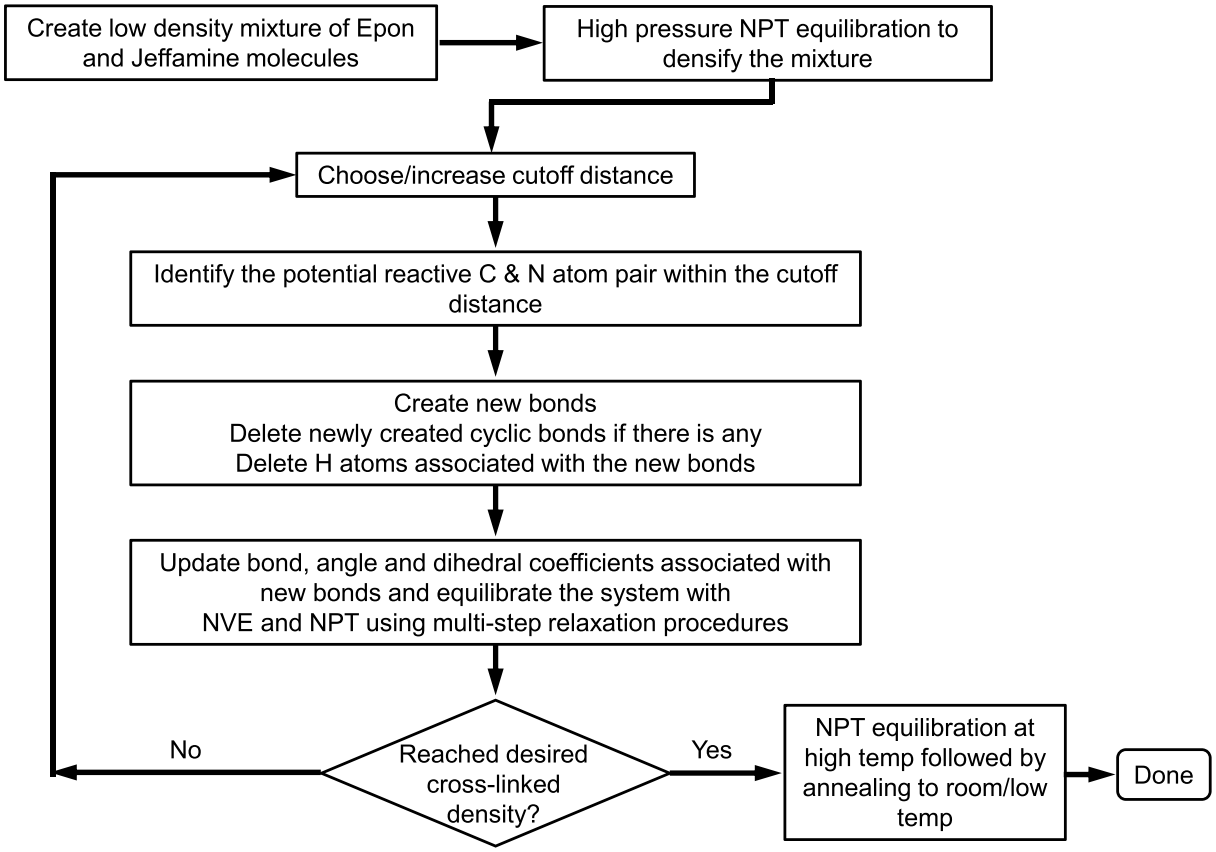

Fig. 3. Flowchart of the cross-link protocol.

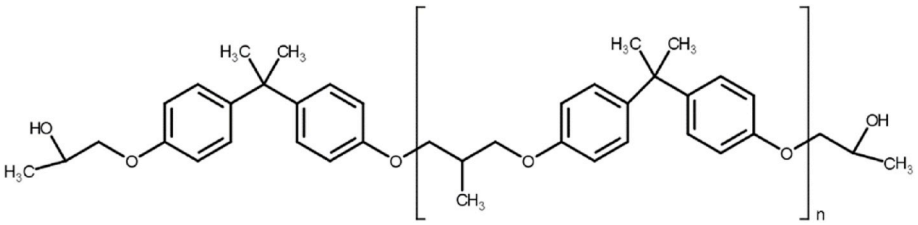

Fig. 4. Molecular structure of hydrogenated Epon molecule.

used in this study, as they have been shown to accurately describe the structure and energetics of epoxy systems [10].

2.2. Model development

To check the effects of the molecular weight (MW) of cross-linker, three cross-linker lengths with index $n = 2.6$, 6.1 and 9.0 which correspond to commercially available cross-linker Jeffamine® D-230, Jeffamine® D-400 and Jeffamine® D-600 are considered. Fig. 1 shows Jeffamine® with Epon 825 molecules. We make these molecules using Arguslab [32]. LAMMPS' [33] compatible topology data are created using Antechamber [14,15], and Moltemplate [14,15] is used to randomly pack these molecules. Table 1a, b provides details on the different molecules with MW and number of molecules used in the three models developed in this study. For convenience, these models are designated as Epon/J230, Epon/J400 and Epon/J600. In all models, Epon with index $n = 0.13$ describes our epoxy resin. Two MWs of Epon with $n = 0$ and $n = 1.0$ molecules are combined in the 6.7:1.0 ratio to get the average index $n = 0.13$. To achieve Jeffamine® index of 2.6, two MWs of Jeffamine with $n = 2$ and $n = 3$ are combined in the 2:3 ratio. Similarly to get Jeffamine® index 6.1, two MWs of Jeffamine® with n = 6 and $n = 7$ are combined in the 9:1 ratio. For Jeffamine® D-600, all molecules with $n = 9$ are considered. The number of molecules meets the stoichiometric ratio 2:1 for Epon and Jeffamine® in all models. To study the degree of cure effects, four average degrees of cure (98.5%, 83.5%, 69.6% and 55.2%) are considered for the Epon/J230 system. Degree of cure is defined as the ratio of reacted epoxide groups to the total epoxide groups. It should be mentioned that due to steric hindrance effects as well as reduction in molecular mobility due to gelation, 100% cross-linking may not be possible to achieve experimentally. Using the FTIR spectroscopy experiments, Jones et al. [34] reported that they achieved 97% (at 70 °C) and 100% (>90 °C) degree of cure for the DGEBA-Jeffamine® D-230 system.

When Epon and Jeffamine® molecules are mixed together in experiments, a cross-linked epoxy structure is formed through the curing reaction between epoxide groups of Epon and amine groups of Jeffamine® molecules. Due to this reaction, Epon and Jeffamine® molecules are connected through C–N bonds (Fig. 2). The reaction cure kinetics are highly dependent on temperature and cure times can span several hundred seconds to hours. This time primarily depends on reactivity and molecular weight of the reactant molecules. In all-atom MD simulations, it is computationally prohibitive to model the curing reaction with these high molecular weight molecules. Therefore, after mixing the Epon and Jeffamine® molecules at stoichiometric ratio in a three-dimensional box, a multi-step cross-link algorithm is used to enforce the cross-link curing reaction by connecting adjacent epoxide and amine groups through C–N bonds. Similar cross-linking methods are available in the literature [6,11]. Fig. 3 shows the protocol/flowchart of the multi-step cross-link algorithm. The following assumptions are made in the cross-link algorithm:

1) Epoxide groups of Epon molecules are hydrogenated (Fig. 4),
2) Both primary and secondary amines have the same reactivity,
3) No etherification reactions and
4) No cyclic reactions (Fig. 5).

The first step of the protocol is to create low density stoichiometric mixture of Epon and Jeffamine® molecules by randomly placing these molecules in a three dimensional cube. The mixture is then densified by equilibrating at high temperature (700 K) and high pressure (200 atm.

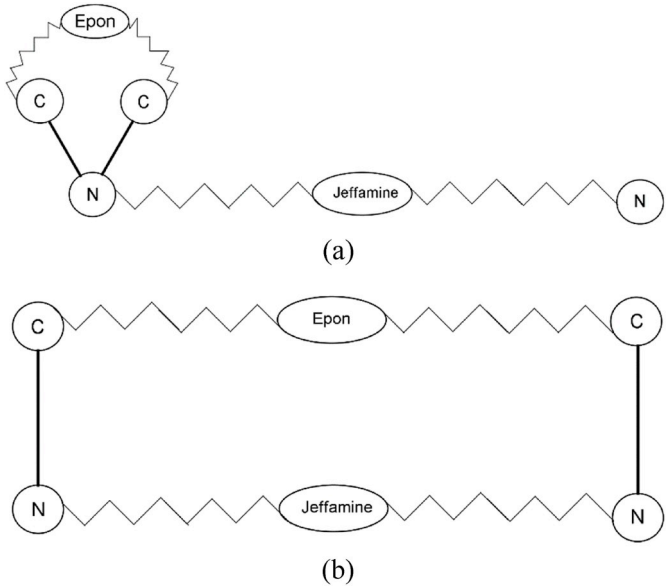

Fig. 5. Schematic of two different types of cyclic reactions.

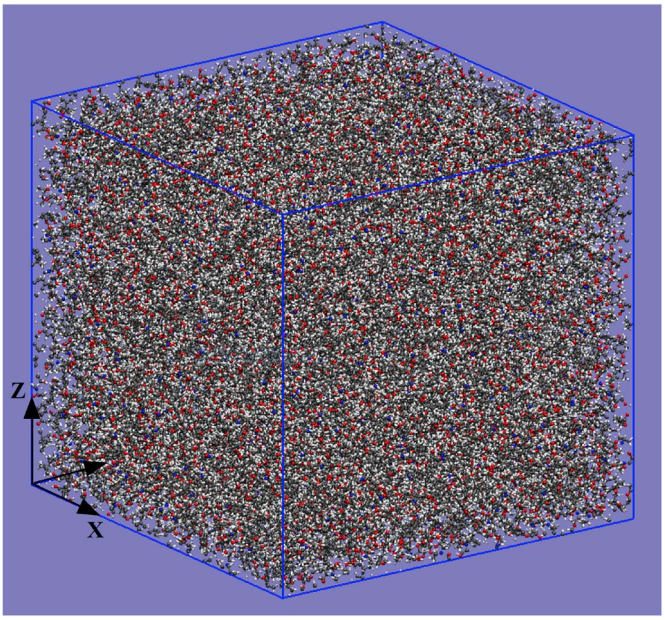

Fig. 6. Cross-linked EPON/J230 epoxy model. VMD [36] is used for visualization purposes.

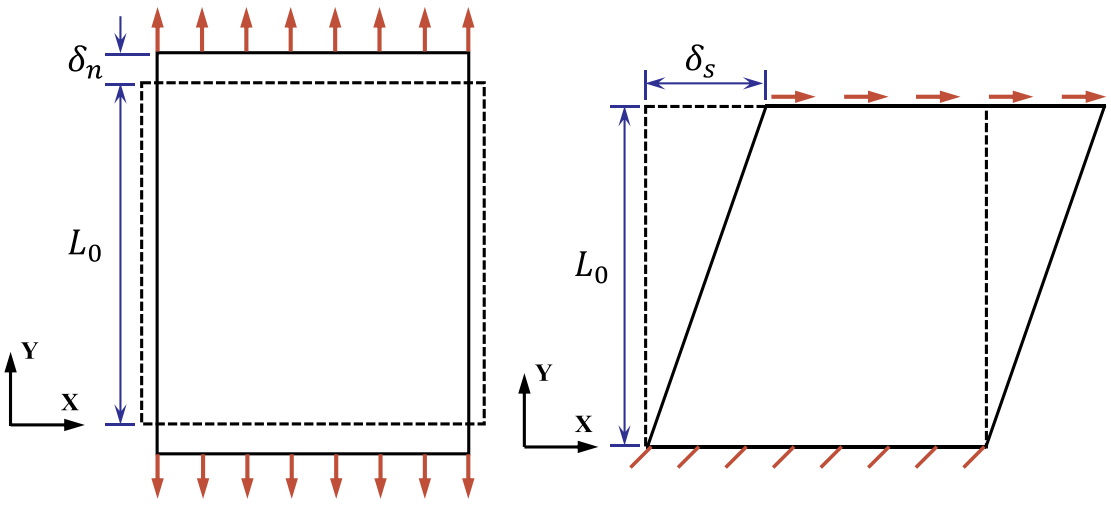

(a) Tensile loading (a) Shear loading

Fig. 7. Loading and boundary condition for (a) tensile and (b) shear loadings.

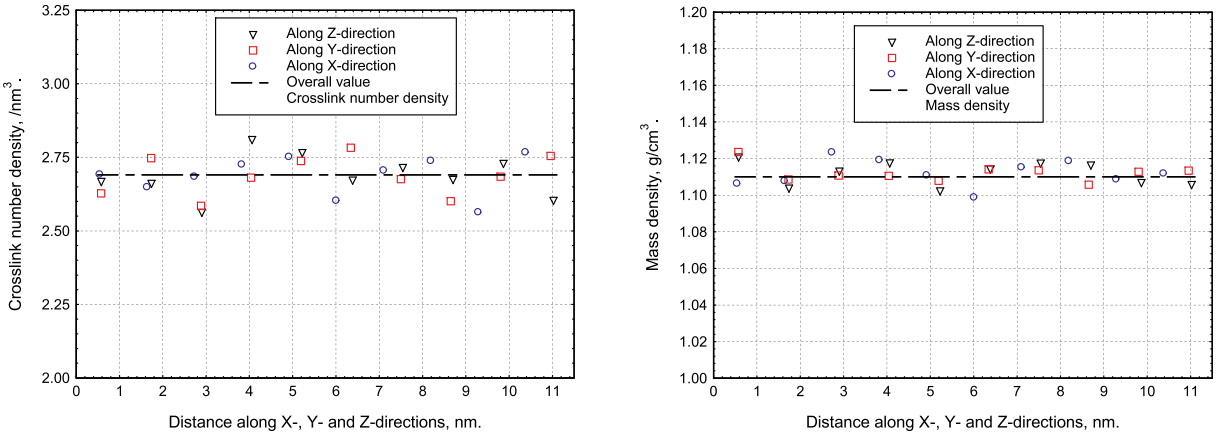

(a) Spatial distribution of degree of cure (a) Spatial distribution of mass density

Fig. 8. Spatial distribution of (a) cross-link and (b) mass density in Epon/J230 model with 98.5% degree of cure.

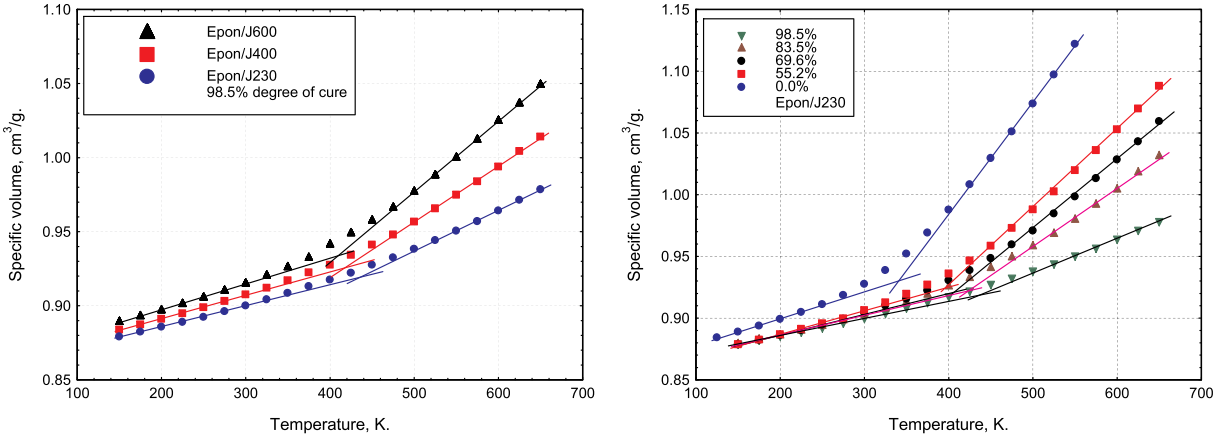

(a) Effects of MW on T_g (a) Effects of degree of cure on T_g

Fig. 9. Variation of specific volume with temperature for (a) models with different MW cross-linker at 98.5% degree of cure and (b) Epon/J230 model with different degree of cure obtained from MD simulations with cooling rate $Q_{sim} = 21.9 \times 10^9\ K/s$. (Data for one replica in each model are shown.)

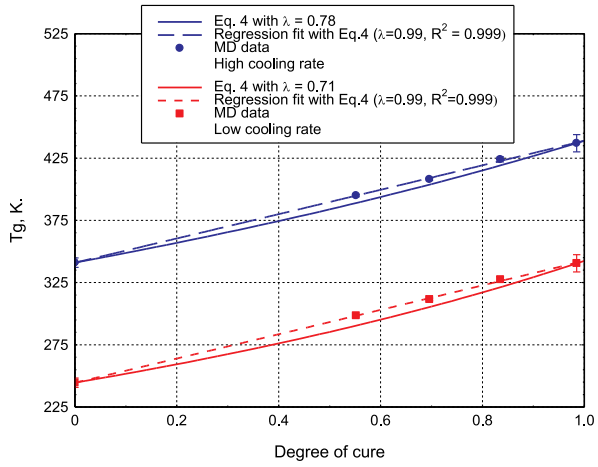

(a) Cooling rate effects (Markers represent MD data)

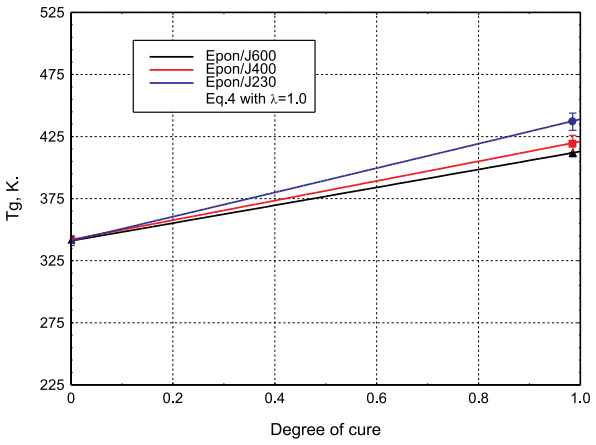

(b) MW effects (Markers represent MD data)

Fig. 10. (a) Variation of T_g with degree of cure for Epon/J230 model at two different cooling rates and (b) effects of the cross-linker MW on the variation of T_g with degree of cure.

pressure) for 0.5 ns and then at room temperature (300 K) and 1 atmospheric pressure for 1 ns using NPT (isothermal-isobaric) ensemble. Atomic interactions are modeled by GAFF with 1 fs time step. Unless and otherwise stated, in all simulations, an equation of motion [35] incorporating a Nosé-Hoover thermostat and anisotropic barostat is used with time constants of 0.1 ps and 1.0 ps, respectively. All MD simulations are carried out with open source molecular simulation software LAMMPS [33]. The second step creates the cross-link reaction where C–N bonds form between C atom of epoxide and N atom of amine groups. The cross-link algorithm searches for the nearest neighbor reactive sites within the search radius and creates C–N bonds. This is implemented by using 'fix bond/create' command available in LAMMPS. Then the system is equilibrated with multi-step relaxation process with NVE (micro--canonical) ensemble for 0.1 ns and NPT (P = 1 atm., T = 300 K) ensemble for 0.1 ns. In the multi-step relaxation process, long bonds are brought to the equilibrium length step by step. We use very low bond stiffness for the long bonds so that the associated atoms do not feel large force and as results the simulation becomes stable. For instance, we use five steps relaxation with stiffness (Kcal/(mol.Å^2)) and length (Å) of (1.0, 10.0), (5.0 7.5), (10.0, 5.0), (20.0 2.5) and (320.6, 1.47) during cross-linking with cutoff distance greater than 1.0 nm. This second step is repeated with an increase in the cutoff search distance until the target degree of cure is reached. To get the 98.5% degree of cure, we start with cutoff distance 0.5 nm and then incrementally increase the cutoff distance by 0.5 nm up to 4.0 nm. To get the 55.2%, 69.6% and 83.5% degree of cure, single step with cutoff 0.56 nm, two steps with cutoff 0.5 nm and 0.7 nm, and two steps with cutoff 0.5 nm and 1.0 nm are used respectively. Incremental cutoff distance is used to avoid frustrated bonds (i.e., long bonds) after equilibration. We do not see long bonds after multi-step relaxation at low degree of cure. However, we find very few long bonds in some models when cutoff distance becomes very large (>3.0 nm). We discard model with long bonds. All of our final models do not have any long bonds. The final step is annealing, where the cross-linked system is heated at high temperature (T = 650 K) using NPT ensemble for 5 ns to remove any residual stress. The system is then cooled to room temperature for further simulation (e.g. mechanical and thermal loading for property and glass transition temperature determination). During cooling, temperature is reduced stepwise with 25 K increments and at each temperature the model is equilibrated for 1 ns. At each temperature step, data was collected during the last 0.25 ns to calculate the specific volume of the model. The glass transition temperature is calculated from the specific volume versus temperature curves which will be discussed later. At the end of this model building procedure, the MD models are sufficiently large (>10 nm in dimension), allowing us to compare results to the literature and capture damage evolution. For each model, three replica structures are created using the above model building procedure.

2.3. Equilibration with ReaxFF

As mentioned earlier, tensile and shear loading simulations are also carried out with reactive force field ReaxFF to understand the atomistic origin of deformation and progressive damage mechanisms. The cross-linked models developed with GAFF are first equilibrated with ReaxFF to reduce any initial internal stress arising from differences in these potentials. At the equilibrium stage, the model is gradually heated from 1 K to 300 K temperature for 250 ps and at 300 K for further 125 ps with NPT ensemble. MD simulation is conducted with time step 0.25 fs and 1 atm pressure. This equilibrated model is then used in tensile and shear simulations with ReaxFF. Fig. 6 shows an equilibrated cross-linked epoxy model. RDF profiles (not shown here) of the GAFF and ReaxFF equilibrated structure are similar and density of the ReaxFF equilibrated structure is slightly higher (see Table 2a) compared to the GAFF.

Table 2a
Effects of MW of cross-linker on mass density at 300 K and Tg obtained with GAFF at 98.5% degree of cure. (Density reported in the parenthesis are obtained with ReaxFF.)

Model Designation	Density (g/cm^3)		Tg (K)	
	MD	Expt.	MD	Expt.
Epon/J230	1.1111 ± 0.0008 (1.205)	1.157 ± 0.001 [4] 1.159 [46]	437 ± 7 328-353*	353-365 [47–49]
Epon/J400	1.1026 ± 0.0009 (1.187)	1.138 ± 0.002 [4] 1.123 ± 0.002 [11]	419 ± 7 310-335*	303 ± 4 [11] 313-325 [47–49]
Epon/J600	1.0924 ± 0.0002 (1.177)	–	411 ± 3 302-327*	–

* MD prediction at the expt. cooling rate obtained with cooling rate correction (Eq. (3)).

Table 2b
Effects of degree of cure on mass density at 300 K and Tg obtained with GAFF for Epon/J230. (Density reported in the parenthesis are obtained with ReaxFF.)

Degree of cure (%)	Density (g/cm^3)	Tg (K)
	MD	MD
98.5	1.1111 ± 0.0008 (1.205)	437 ± 7 328-353*
83.5	1.1078 ± 0.0015 (1.189)	424 ± 2 315-340*
69.6	1.1070 ± 0.0005 (1.185)	408 ± 1 299-324*
55.2	1.1045 ± 0.0002 (1.180)	395 ± 1 286-311*
0.0	1.0782 ± 0.0001	341 ± 4 232-257*

* MD prediction at the expt. cooling rate obtained with cooling rate correction (Eq. (3)).

2.4. Boundary and loading conditions for tensile loading

Epoxy formulations are isotropic. To apply a uniaxial tensile load, the model is subjected to uniform tensile strain in a specific direction (i.e., either X or Y or Z direction) as shown in Fig. 7a. The solution domain is linearly expanded with a constant axial strain/displacement rate by scaling the coordinates of all atoms along the specific direction at every time step followed by MD time integration [37–39]. To mimic the plane-stress condition, transverse direction movements due to Poisson's effect are allowed (i.e. zero net force in these directions). MD time step 1 fs for GAFF and 0.25 fs for ReaxFF are used and NPT ensemble with temperature 300 K and pressure 1 atm. is considered. Strain rate used in the tensile simulations is $5.0 \times 10^9 s^{-1}$ and periodic boundary is applied in all directions.

Stress is calculated using the classic definition of virial stress [40–42].

$$\sigma_{ij}^{V} = -\frac{1}{V}\sum_{\alpha=1}^{N}\left[m_\alpha v_i^\alpha v_j^\alpha + \frac{1}{2}\sum_{\beta\neq\alpha} r_{ij}^{\alpha\beta} f_{ij}^{\alpha\beta}\right] \quad (1)$$

Where V is the model volume, N is the number of atoms in the model, m is the mass of atom, v is the velocity of atom, r is the inter-atomic distance and f is the inter-atomic force. The subscripts i and j stand for X, Y and Z directions values. The above virial stress corresponds to true stress. Engineering stress is determined by scaling the virial true stress with the initial cross-section area of the model. Engineering stress and strain are defined using the following formula

$$\sigma = \frac{\sigma_{ij}^{V} \times A}{A_0} \quad (2a)$$

$$\varepsilon = \frac{\delta_n}{L_0} = \frac{L - L_0}{L_0} \quad (2b)$$

Where A is the instantaneous cross-section area, A_0 is the initial cross-section area, L_0 is the initial model length and L is the current model length.

2.5. Boundary and loading conditions for shear loading

Simple shear deformation [43] is applied in a specific direction by scaling the corresponding position component of all atoms followed by MD time integration [39] as shown in Fig. 7b. NVT ensemble with temperature 300 K is used in the simulations. The shear strain rate used in the shear loading is $1.0 \times 10^{10} s^{-1}$. Shear stress is calculated from virial formula (Eq. (1)) and shear strain is determined from the ratio of shear displacement (δ_s) to the model length (L_0) perpendicular to the shear direction [44,45].

3. Results and discussion

3.1. Properties of structure

To analyze the structure of the cross-linked epoxy network, we determine spatial distribution of cross-links (i.e., C–N bonds density), spatial distribution of mass density and overall mass density for different models obtained after equilibration at 300 K with GAFF. To determine spatial distribution, the model is split into several divisions with equal thickness in three orthogonal X-, Y- and Z-directions. Spatial cross-link and spatial mass density are determined by dividing the total number of cross-link C–N bonds and total atomic mass available in a specific division with the volume of the corresponding division. Fig. 8 shows spatial distribution along three directions for Epon/J230 model at 98.5% degree of cure. Both the cross-link and mass density fluctuates around overall system density indicating that the created epoxy network structure is homogeneous. Variation of mass density for different models are shown in Table 2 along with T_g (which will be discussed in the next section). In case of GAFF, average properties with standard deviation are obtained from three replicas while in case of ReaxFF average properties are obtained from two replicas. Model with shorter cross-linker

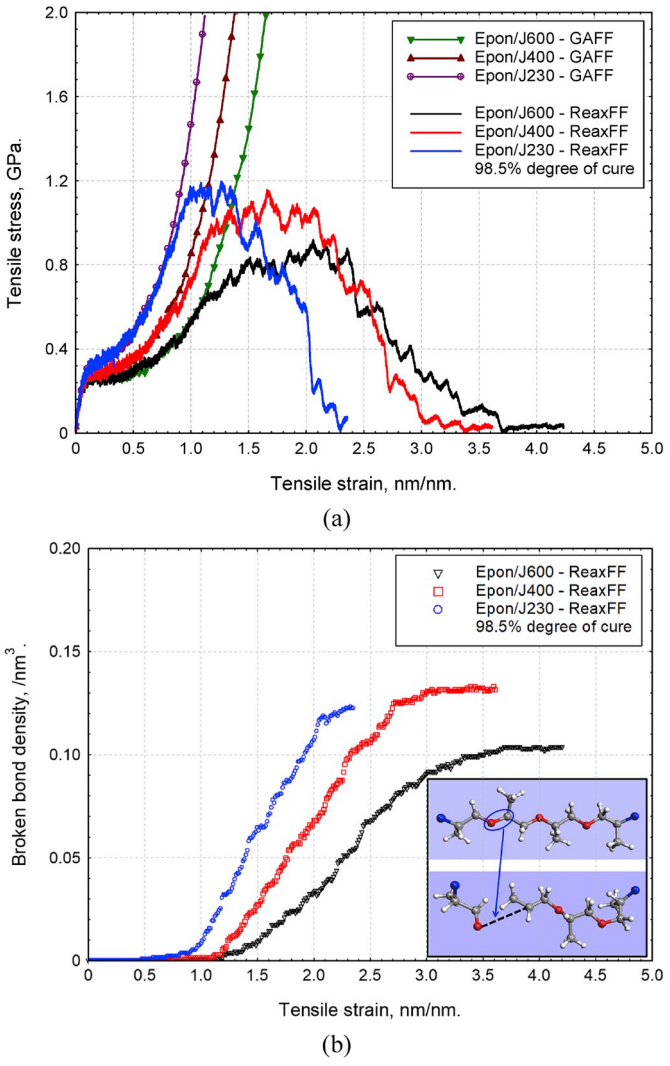

Fig. 11. (a) Effects of cross-linker MW on the tensile stress-strain obtained with GAFF and ReaxFF with strain rate $5.0 \times 10^9 s^{-1}$. (b) Variation of broken bonds with strain obtained with ReaxFF. Data for one replica in each model are shown for comparison (Inset in Fig. 11b shows breakage of C–O bond in Jeffamine® cross-linker.).

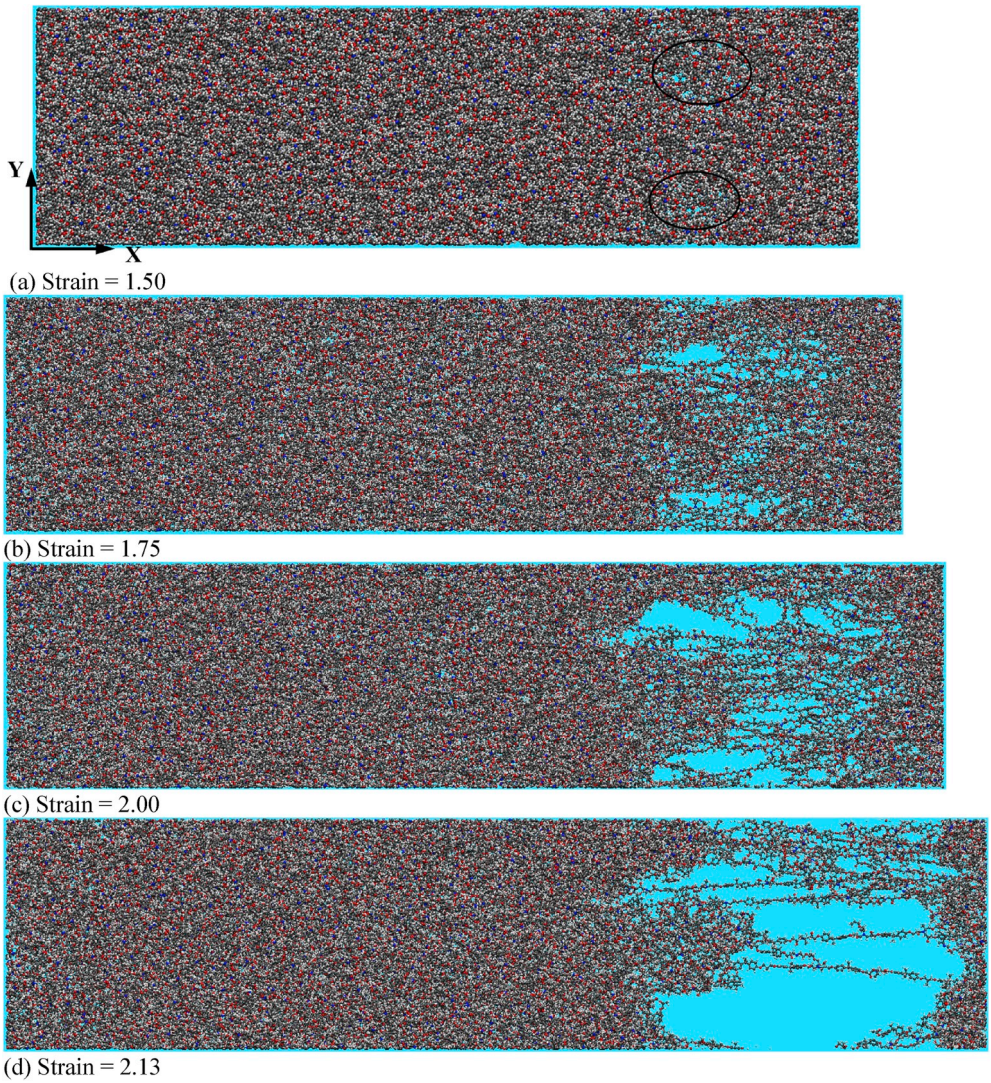

Fig. 12. Progressive damage of Epon/J230 model with 98.5% degree of cure under X-direction tension obtained with ReaxFF. (Black oval marks in Fig. 12a show damage area).

molecules and higher degree of cure has higher density due to the closely packed network structures. The densities obtained from MD simulations are in reasonable agreement with experiments, considering that the experimental values lie between the GAFF and ReaxFF densities. Mass density and thermo-mechanical properties (shown later) obtained with GAFF agree well with the previous MD simulations [8,11].

3.2. Glass transition temperature T_g

Glass transition temperature (T_g) is a key thermal property of epoxy resins which limits its service temperature. Glass transition temperature is calculated from the specific volume versus temperature curves. Fig. 9 shows the variation of the specific volume with temperature for the 98.5% cross-linked Epon/J230 model. The resin is in the rubbery and glassy state at high and low temperature. Therefore, the temperature profile shows two distinct slopes at the high (T > 500 K) and low (T < 300 K) temperature regions. T_g is determined from the intersection of the two slopes. Table 2 shows T_g values for different models. The overall trend is that the epoxy with longer cross-linker and lower degree of cure has lower T_g value. Longer cross-linker molecules are less rigid (i.e., mobility is higher at thermal excitation) compared to the shorter cross-linker molecules. Experimental measurements also exhibit this trend [47–49]. However, MD simulation values are higher than experimental values which is due to the higher cooling rate used in the simulations.

The effects of cooling rate on T_g has been shown experimentally to follow the Williams-Landel-Ferry (WLF) equation [50]:

$$\Delta T_g = \frac{-C_2 log_{10}(Q_{exp}/Q_{sim})}{C_1 + log_{10}(Q_{exp}/Q_{sim})} \quad (3)$$

Where ΔT_g is the shift in glass transition temperature due to difference in experimental and simulation cooling rates Q_{exp} and Q_{sim}. For the universal values of WLF parameters $C_1 = 17.44$, $C_2 = 51.6\,K$ [50], $Q_{sim} = 21.9 \times 10^9\,K/s$ and $Q_{exp} = 0.033 - 0.33\,K/s$ [8], ΔT_g is in the range of 84 K–109 K. Applying this cooling rate correction to the MD simulations results in good correlation with the experimental values measured under low cooling rates. In one recent study, Khare et al. [51] have also shown that the WLF equation with material specific constants also provided good correlation with experiments after the simulation data is corrected.

As shown in Table 2b and Fig. 9b, the glass transition temperature increases with the increase in the degree of cure. At approximately a degree of cure of 55%, the glass transition temperature is equal to room

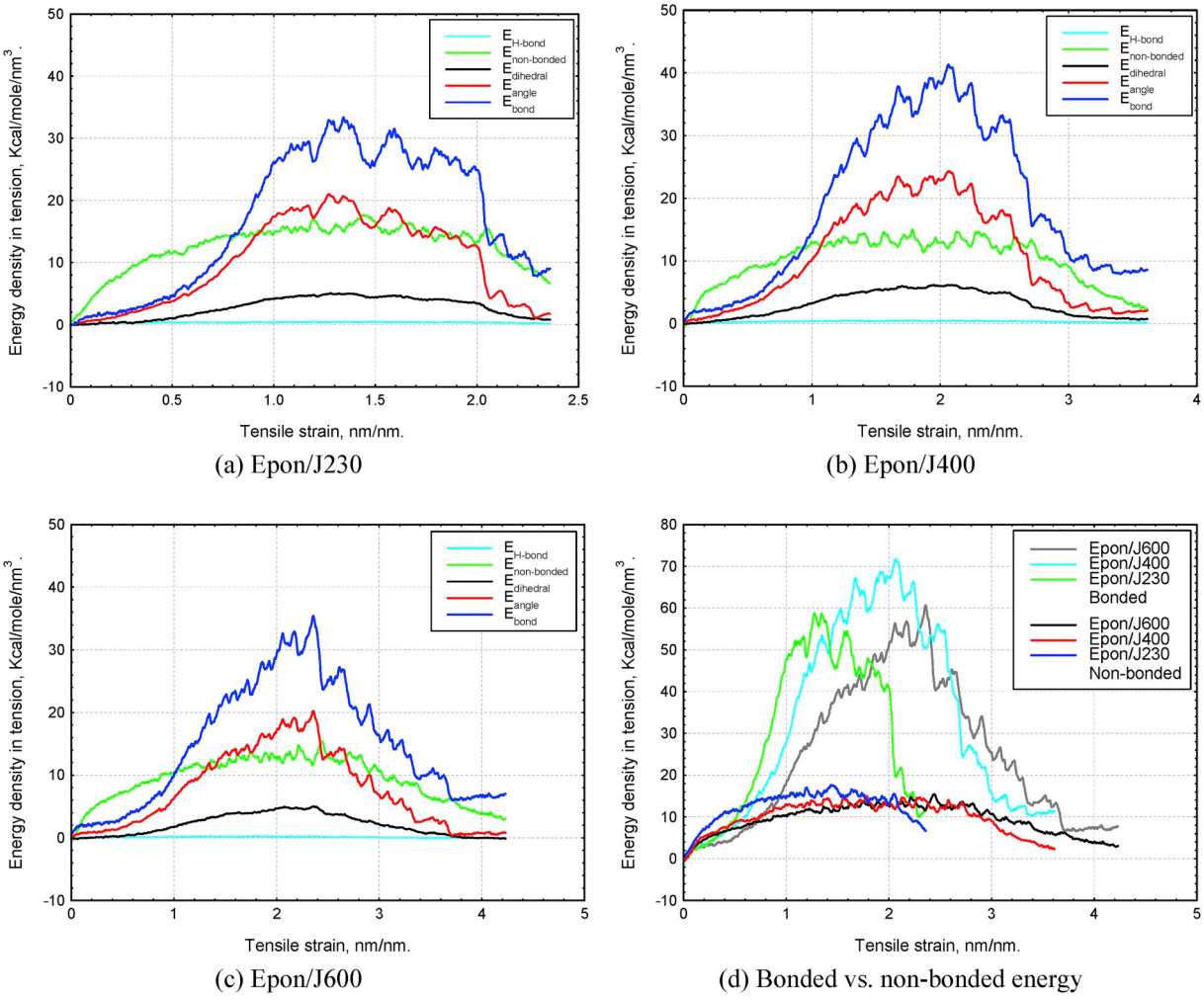

Fig. 13. Effects of MW of cross-linker on the bonded and non-bonded energy in tension. (Data for one replica in each model are shown.)

temperature which implies that this Epon resin is approximately at gel state at lower degree of cure which is true for this system.

The DiBenedetto Equation (Eq. (4)) [52] is widely used to predict the relationship between T_g and degree of cure (X).

$$\frac{T_g(X) - T_g(0)}{T_g(\infty) - T_g(0)} = \frac{\lambda X}{1 - (1 - \lambda)X} \tag{4}$$

Here $T_g(0)$ and $T_g(\infty)$ are the glass transition temperature of uncured and fully cured resin and λ is an empirical parameter approximated as [53]:

$$\lambda = \frac{T_g(0)}{T_g(\infty)} \tag{5}$$

Using the results presented in Table 2b for the Epon/J230, λ based on Equation (5) is 0.71–0.78. MD predictions for T_g as a function of degree of cure is given in Table 2b along with the corrected low cooling rate values. Fig. 10a shows the variation of T_g with the degree of cure for Epon/J230 at both cooling rates. A regression fit of the full DiBenedetto relationship in Equation (4) to the MD results for each cooling rate gives $\lambda = 0.99$ with R^2 value of 0.999 and $T_g(\infty)$ value at 100% degree of cure is 2 K higher than that of 98.5% degree of cure. This proves that the variation of T_g with degree of cure is linear for the Epon/J230 system and that $\lambda = 1$ should be used in the DiBenedetto relationship (Equation (4)). For comparison purposes the DiBenedetto Equation is also plotted (solid lines in Fig. 10a) with the λ calculated from the T_g ratio (i.e., $\lambda = \frac{T_g(0)}{T_g(\infty)}$). This approach underestimates the glass transition temperatures at intermediate degree of cure compared to the MD prediction with a maximum difference of 5 – 8 K. Fig. 10b shows the effects of cross-linker MW on the variation of T_g with degree of cure plotted with DiBenedetto Equation using $\lambda = 1$. At a particular degree of cure, T_g is higher for the lower MW cross-linker due to the higher cross-link density.

3.3. Tensile stress-strain response and failure mechanism

Fig. 11a shows the effects of the MW of cross-linker on the tensile stress-strain response obtained with GAFF and ReaxFF for 98.5% degree of cure models. Stress-strain curves show four distinct regions – initial linear response, yielding (i.e., plateau stress level), strain hardening and progressive failure. GAFF and ReaxFF predictions agree well up to the strain where material starts to fail through bond breakage. At larger strains, GAFF predicts dramatic stiffening and unrealistic high stress levels as bonds stretch without breakage while ReaxFF shows realistic progressive damage and energy absorption. The strain limit up to which GAFF prediction agrees with ReaxFF depends on cross-linker length and degree of cure. At 98.5% degree of cure, GAFF prediction is limited to 75–110% strain levels but it cannot accurately predict tensile strength and energy absorption. Fig. 11 provides guidance on the limits of applicability of the GAFF potential based on the strains at which bond

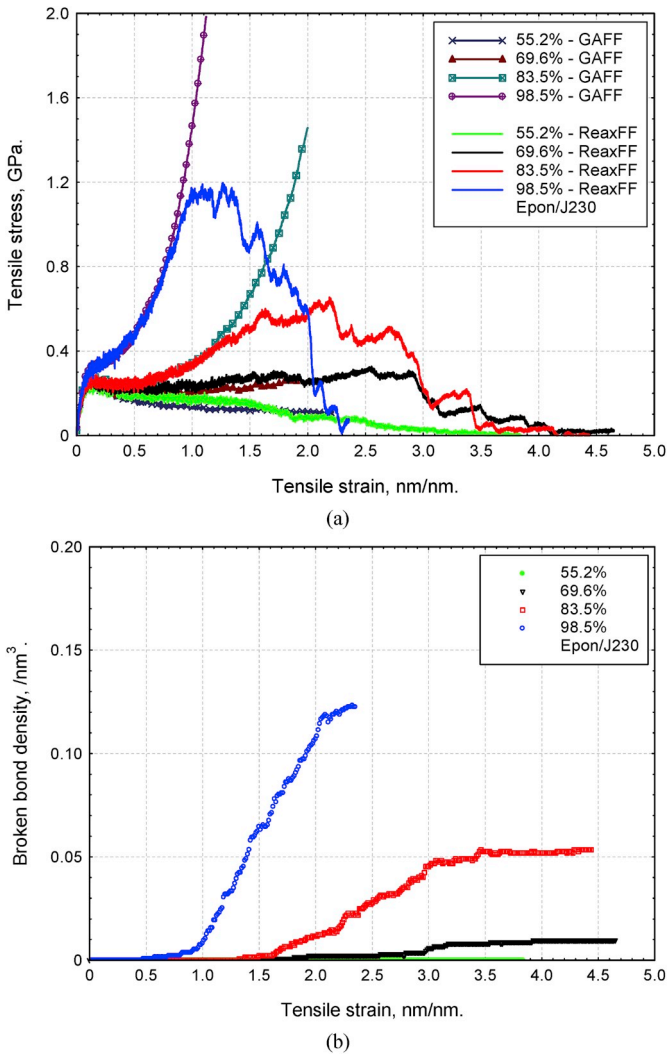

Fig. 14. Effects of degree of cure on the tensile stress-strain response obtained with GAFF and ReaxFF for Epon/J230 system with strain rate $5.0 \times 10^9 s^{-1}$. (b) Variation of broken bonds with strain obtained with ReaxFF for the same systems. (Data for one replica in each model are shown.)

breakage initiates.

To understand the deformation mechanisms at different stages of loading, major energy contributions from bond, angle, dihedral, non-bonded vdW and columbic interactions, H-bonds as well as broken bond data during ReaxFF simulations are monitored. Fig. 11b shows evolution of broken bonds with tensile strain for the three systems. ReaxFF bond order cutoff 0.30 is used in LAMMPS to identify broken bonds. Usually the C–O bond in the cross-linker molecules (shown in the inset in Fig. 11b) and C–N bond either in the epoxide-amine reaction junction or in the cross-linker fails. To explore why these specific bonds fail, we perform bond stretching analysis of the key bonds which are present in the backbone of an Epon-Jeffamine® molecule. We consider Ethane, Methylamine, Methanol and Phenol molecules. First we equilibrate these molecules and then stretch the C–C bonds in Ethane, C–N bond in Methylamine, C–O bond in Methanol and C–O bond in Phenol along the corresponding bond axis with ReaxFF. Figs. A1-A2 in Appendix A show the force-displacement and energy-displacement responses and bond peak force and energy are summarized in Table A1 in Appendix A. Bond stretching analysis shows that the C–O and C–N bonds have low failure force (6.5 nN for C–N and 8.2 nN for C–O bond).

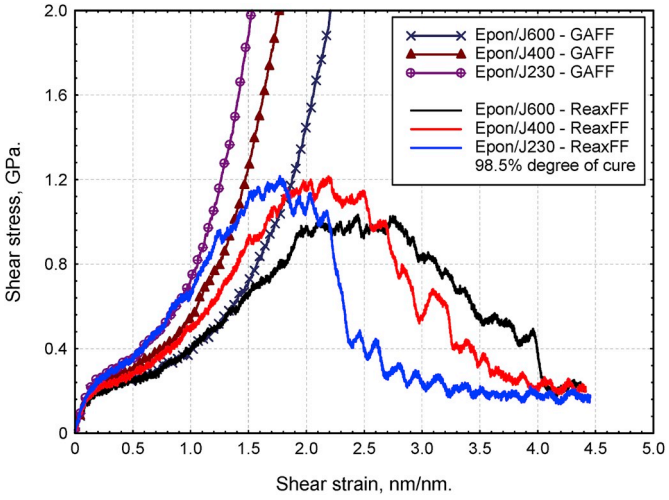

Fig. 16. Effects of cross-linker MW on the shear stress-strain obtained with GAFF and ReaxFF with strain rate $1.0 \times 10^9 s^{-1}$. (Data for one replica in each model are shown.)

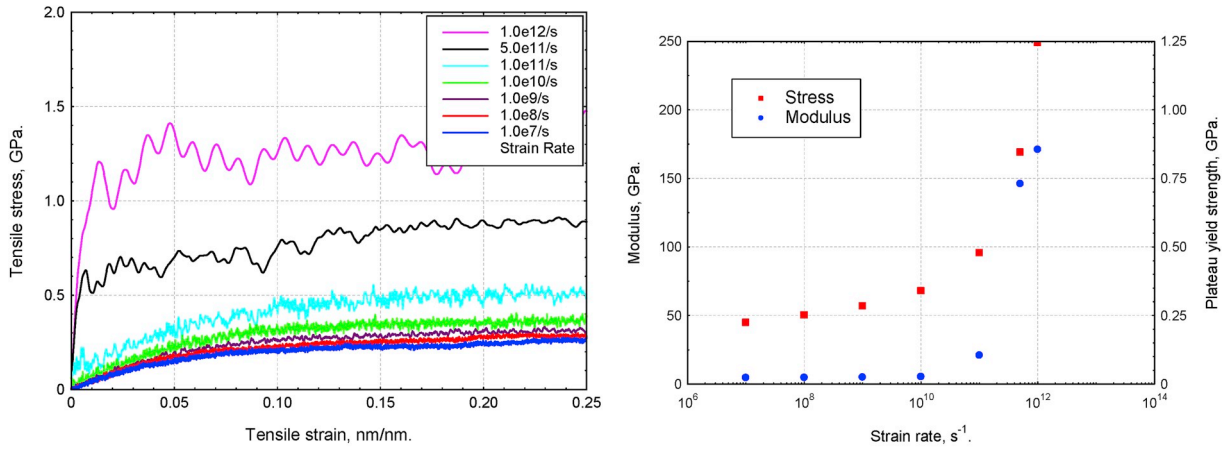

Fig. 15. Effects of strain rate on the tensile (a) stress-strain response and (b) modulus and yield strength obtained with GAFF for Epon/J230 with 98.5% degree of cure.

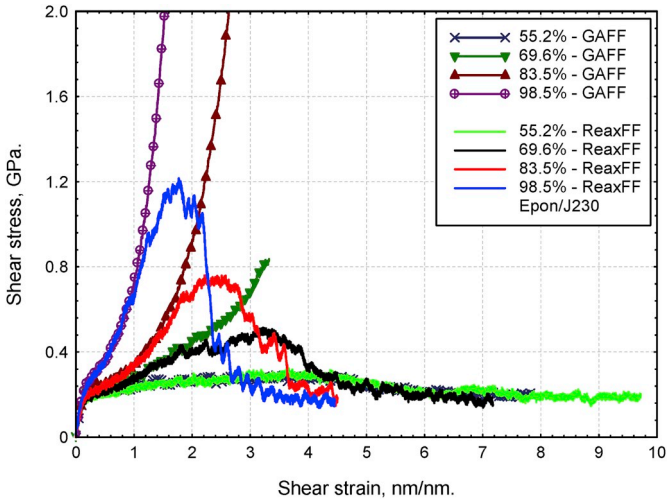

Fig. 17. Effects of degree of cure on the shear stress-strain obtained with GAFF and ReaxFF for Epon/J230 system with strain rate $1.0 \times 10^9 s^{-1}$. (Data for one replica in each model are shown.)

Consequently, these bonds fail during mechanical loadings of the cured epoxy system. Very few bonds break in the strain hardening region. Bond breakage starts to increase at the end of strain hardening (ε=100% in Epon/J230, $\varepsilon = 135\%$ in Epon/J400 and $\varepsilon = 150\%$ in Epon/J600). As the loading continues, bonds gradually start to fail and stress remains almost in the plateau level for a certain time and strain increment and then reduces. This is analogous to the progressive damage in the continuum length scale. Bond breakage curves are sigmoidal – rate of bond breakage starts at zero, increase to maximum value at the strain where stress starts to drop ($\varepsilon = 150\%$ for Epon/J230, $\varepsilon = 190\%$ for Epon/J400 and $\varepsilon = 226\%$ for Epon/J600) and then decreases to zero at large strain. Bond breakage evolves into voids and fibrillary structure leading to complete failure as shown in Fig. 12. Very few bonds break in the strain hardening region giving a local drop in the stress without affecting the overall stress-strain response.

ReaxFF energy data for the same three systems with 98.5% degree of cure are shown in Fig. 13a–c and comparison of the bonded (bond + angle + dihedral) and non-bonded (vdW + coulomb) energy is shown in Fig. 13d. For each types of energy, energy difference (ΔE) from the reference energy at 0% strain is considered. Non-bonded interaction dominates within the linear and yield regions while the bonded interaction starts to pick up at larger strains within the strain hardening region. H-bond interaction has insignificant energy contribution due to the lack of polar OH and NH groups in the cured epoxy system. As shown in Fig. 13d, non-bonded interaction is more prominent in case of shorter MW cross-linker at low strain range giving high modulus and yield strength (reported later). At high strain near the peak force, bond stretching and the associated angle and dihedral deformation absorb significant amounts of energy.

Effects of degree of cure on the tensile stress-strain responses are shown in Fig. 14a for the Epon/J230 system and the corresponding broken bond data are shown in Fig. 14b. ReaxFF energy data for 83.5%, 69.6% and 55.2% degree of cure models are shown in Figs. B1a-B1c in Appendix B for completeness. With the decrease in degree of cure, strain hardening region disappears in the stress-strain curves (Fig. 14a) and non-bonded interaction energy dominates throughout the entire loading (Fig. B1b & B1c). Number of broken bonds decreases as degree of cure decreases and no bond breakage is observed in case of 55.2% degree of cure (Fig. 14b). At 55.2% degree of cure, epoxy structure has some uncured regions randomly distributed throughout the system. Under deformation, the system fails at these regions through the separation of uncured molecules without bond breakage.

Table 3a
Effects of MW of cross-linker on the tensile properties for 98.5% degree of cure obtained with strain rate $5.0 \times 10^9 s^{-1}$ at 300K. Values reported in the parenthesis are obtained with ReaxFF.

Model Designation	Modulus (GPa)		0.2% Offset Yield Strength (GPa)	Plateau Yield Strength (GPa)	Ultimate Strength (GPa)	Energy (GJ/m^3)
	MD	Expt.	MD	MD	MD	MD
Epon/J230	4.91 ± 0.19 (5.29)	2.36 ± 0.07 [4]	0.187 ± 0.007 (0.170)	0.345 ± 0.017 (0.324)	(1.143)	(1.66)
Epon/J400	4.76 ± 0.23 (4.74)	2.37 ± 0.11 [4] 2.36 ± 0.23 [11]	0.171 ± 0.010 (0.172)	0.300 ± 0.008 (0.290)	(1.090)	(1.89)
Epon/J600	4.57 ± 0.14 (4.61)	2.36 ± 0.07 [4]	0.175 ± 0.010 (0.158)	0.269 ± 0.006 (0.259)	(0.885)	(1.82)

Tensile mechanical properties are tabulated in Table 3. The modulus is determined from linear regression in the initial linear stress-strain portion (<2% strain). The yield strength is determined using both 0.2% offset method and from the plateau stress. Stress-strain responses show plateau stress near 10% strain in between the linear and strain hardening regions (Figs. 11a and 14a) where the stress gradient becomes zero. It should be mentioned that this plateau stress is also considered as yielding state of materials [24,54]. In case of ReaxFF simulations, ultimate strength is determined from the peak stress and total absorbed energy is obtained from the area under the stress-strain curve. To determine the average values with standard deviation in GAFF simulations, three replicas of all models are loaded in the three orthogonal directions. For ReaxFF simulation, average data are obtained from two simulations of two replicas. Models with higher MW cross-linker and lower degree of cure give lower modulus, plateau stress and tensile strength. Yield strength obtained with 0.2% offset method doesn't show any specific trend. The cross-linkers become less rigid with the increase in their MW. This low rigidity cross-linker reduces the stiffness and strength of the epoxy. In case of low degree of cure, there are sufficient

Table 3b
Effects of degree of cure on the tensile properties for Epon/J230 model obtained with strain rate $5.0 \times 10^9 s^{-1}$ at 300K. Values reported in the parenthesis are obtained with ReaxFF.

Degree of cure (%)	Modulus (GPa)	0.2% Offset Yield Strength (GPa)	Plateau Yield Strength (GPa)	Ultimate Strength (GPa)	Energy (GJ/m^3)
	MD	MD	MD	MD	MD
98.5	4.91 ± 0.19 (5.29)	0.187 ± 0.007 (0.170)	0.345 ± 0.017 (0.324)	(1.143)	(1.66)
83.5	4.69 ± 0.21 (5.03)	0.167 ± 0.005 (0.143)	0.274 ± 0.008 (0.260)	(0.670)	(1.32)
69.6	4.58 ± 0.24 (4.72)	0.167 ± 0.008 (0.147)	0.260 ± 0.007 (0.254)	(0.300)	(0.96)
55.2	4.50 ± 0.12 (4.54)	0.158 ± 0.009 (0.134)	0.252 ± 0.006 (0.235)	(0.236)	(0.44)

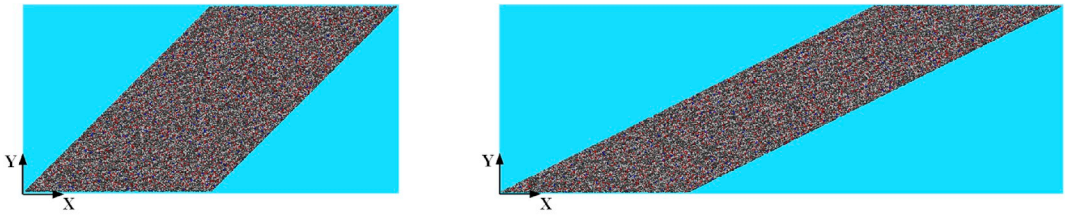

(a) Shear strain = 1.0 (b) Shear strain = 2.0

Fig. 18. Shear deformation of Epon/J230 epoxy system with 98.5% degree of cure with ReaxFF.

amount of non-bonded free molecules which are embedded inside the system, however, they do not contribute much to the mechanical response. Therefore, it could be postulated that epoxy with larger MW cross-linker and low degree of cure would give lower stiffness and strength. Conversely, with the 62% decrease in the cross-linker MW (i.e., from $MW = 598.4$ g/mol for Jeffamine® D-600 to $MW = 225.7$ g/mol for Jeffamine® D-230), tensile modulus, plateau yield strength and ultimate strength increase by 7–15%, 25–28% and 29% respectively. Similarly, with the increase of degree of cure from 55% to 98.4%, tensile modulus, plateau yield strength and ultimate tensile strength increase by 9–17%, 39–46% and 384% respectively. This suggests elastic modulus is less affected by the cross-linker length and degree of cure since mechanical deformation is mainly controlled by the non-bonded interaction and not by the bonded interaction at low strain level as discussed earlier. Total absorbed energy is not significantly affected by the cross-linker MW for the highest degree of cure system (i.e. 98.5%). Although the smaller MW cross-linker system has reduced failure strain, this potential reduction in absorbed energy is offset by its higher yield stress and high stiffness strain hardening response (Table 3a). However, absorbed energy decreases significantly with decrease in the degree of cure for all MW cross-linkers as shown in Table 3b.

MD predicted properties are higher than the experimental values which can be attributed to the high strain rate and nano-scale structure with no larger length scale defects included in the MD simulations. The strain rate dependent stress-strain response and the strain rate effect on the modulus and yield strength are presented in Fig. 15 for the Epon/J230 system at 98.5% cure. The modulus and plateau yield strength increase significantly with strain rate, as expected [55]. For example, a 100-fold increase in strain rate (10^{10} to 10^{12} s-1) increases the plateau stress by a factor of 4, similar to the behavior reported in an epoxy resin by Tamrakar et al. [54,56]. Likewise, the yield stress versus strain rate shown in Fig. 15b follows a bi-linear relationship on a semi-log scale that resembles previous results for a DER 353 epoxy [54,56]. We note that the MD predicted properties are significantly higher than experimental values. For example, the modulus of Epon/J230 has been reported as 2.4–2.8 GPa [4,11,57], whereas our predicted value is nearly 5 GPa (Table 3). The reason for this discrepancy is the ballistic strain rate employed in our simulations ($\geq 10^7$ Hz), compared to the quasi-static experimental strain rate ($\sim 10^{-3}$ Hz in Refs. [4,11,57]). As shown in Fig. 15, the modulus and strength increase significantly as the strain rate is raised. Thus, our results are best viewed in the context of ballistic strain rates. An in-depth study on strain rate effects on the visco-elastic-plastic stress-strain response and failure mechanisms will be the topic of future work.

3.4. Shear stress-strain response and failure mechanism

Effects of MW of cross-linker and degree of cure on the shear stress-strain response are shown in Figs. 16 and 17. Like tensile response, shear stress-strain curves also show linear, yield, strain hardening and failure regions. Strain-hardening region disappears with the decrease in degree of cure (Fig. 17). GAFF and ReaxFF curves agree well up to strain hardening regions (90–135% strain) for 98.5% cross-link models. At higher shear strain, bond breakage commences and GAFF stiffens unrealistically and cannot accurately predict strength and energy absorption. However, they agree well throughout the entire loading curves for low degree of cure systems (i.e., 55.2% degree of cure shown in Fig. 17) since there is no bond breakage. Epoxy with low degree of cure (55.2%) behaves more like a viscous material (Fig. 17) since the T_g (corrected value) of this resin is close to the room temperature and the resin would be in liquid state near the room temperature.

Table 4a
Effects of MW of cross-linker on the shear properties for 98.5% degree of cure obtained with strain rate $1.0 \times 10^9 s^{-1}$ at 300K. Values reported in the parenthesis are obtained with ReaxFF.

Model Designation	Modulus (GPa)		0.2% Offset Yield Strength (GPa)	Plateau Yield Strength (GPa)	Shear Strength (GPa)	Energy (GJ/m^3)
	MD	Expt.	MD	MD	MD	MD
Epon/J230	1.96 ± 0.06 (1.98)	1.09 ± 0.01 [60]	0.153 ± 0.014 (0.130)	0.259 ± 0.009 (0.250)	(1.18)	(2.25)
Epon/J400	1.91 ± 0.11 (1.88)	1.01 ± 0.01 [60]	0.139 ± 0.012 (0.121)	0.250 ± 0.006 (0.220)	(1.17)	(2.47)
Epon/J600	1.82 ± 0.10 (1.79)	–	0.129 ± 0.009 (0.091)	0.233 ± 0.008 (0.197)	(0.96)	(2.50)

Table 4b
Effects of degree of cure on the shear properties for Epon/J230 model obtained with strain rate $1.0 \times 10^9 s^{-1}$ at 300K. Values reported in the parenthesis are obtained with ReaxFF.

Model Designation	Modulus (GPa)	0.2% Offset Yield Strength (GPa)	Plateau Yield Strength (GPa)	Shear Strength (GPa)	Energy (GJ/m^3)
	MD	MD	MD	MD	MD
98.5	1.96 ± 0.06 (1.98)	0.153 ± 0.014 (0.130)	0.259 ± 0.009 (0.250)	(1.18)	(2.25)
83.5	1.82 ± 0.06 (1.80)	0.126 ± 0.008 (0.108)	0.252 ± 0.005 (0.206)	(0.77)	(1.92)
69.6	1.79 ± 0.09 (1.74)	0.129 ± 0.008 (0.094)	0.232 ± 0.004 (0.193)	(0.48)	(1.71)
55.2	1.75 ± 0.08 (1.62)	0.124 ± 0.004 (0.111)	0.224 ± 0.003 (0.182)	(0.29)	(1.49)

Energy partitioning curves are shown in Fig. B2 in Appendix B for different cross-linker MW and degree of cure. Like the tensile loading, shear deformation is also controlled by the non-bonded interaction at low strain. However, non-bonded interaction dominates throughout the entire loading in case of low degree of cure (Fig. B2f). Damage initiates through bond breakage (broken bonds data is not shown), but due to the nature of loading it is hard to visualize these damage areas in the shear deformed amorphous structure (Fig. 18). Even after failure, damage surfaces slide over each other giving a constant shear reaction of about 0.18 GPa at large strain (>400% strain) as shown in Figs. 16 and 17. This behavior has been observed in the micro-droplet test after interphase debonding under shear deformation [58].

Corresponding shear mechanical properties are reported in Table 4. Plateau yield stress is calculated around 20% shear strain. To calculate the absorbed energy in shear, stress-strain curve is integrated up to the strain limit where stress reaches the plateau value 0.18 GPa. Shear modulus, plateau yield strength and ultimate strength increase by 8–11%, 11–27% and 23% for 62% decrease in the cross-linker MW (i.e., from $MW = 598.4$ g/mol for Jeffamine® D-600 to $MW = 225.7$ g/mol for Jeffamine® D-230). Whereas modulus, yield strength and ultimate strength increase by 12–22%, 16–37% and 307% for increase in the degree of cure from 55.2% to 98.5%. Absorbed energy in shear is not significantly affected by the cross-linker MW, however, absorbed energy decreases monotonically with decrease in the degree of cure.

As we noticed in the shear loading MD simulations, normal stress develops (not shown here) in the shear direction (i.e., normal stress in the X-direction develops in case of the XY-plane shear loading) which is also reported in Ref. [59]. This means simple shear load creates combined effects of shear as well as tension at large deformation. At ultimate strength, the same type of bonds break in shear and tensile loading, therefore, tension and shear give the same ultimate strength. Yield strength ratio (i.e., shear yield strength/tensile yield strength) varies between 0.73 and 0.92, indicating ductile behavior of the epoxy resins. Poisson's ratio calculated from tensile simulations are in the range of 0.25–0.29 (GAFF) and 0.30–0.41 (ReaxFF) and it follows the isotropic relation $G = E/2(1+\nu)$ at small strains linear region below yield.

4. Conclusions

All-atom molecular dynamics (MD) simulations are conducted to study the effects of the molecular weight (MW) of Jeffamine® cross-linker and degree of cure on the structure and thermo-mechanical properties of Bisphenol A diglycidyl ether (Epon 825) epoxy resin. Three MWs for cross-linker (Jeffamine® D-230, Jeffamine® D-400 and Jeffamine® D-600) and four degrees of cure (98.5%, 83.5%, 69.6% and 55.2%) are considered. Cross-linked networks are created from stoichiometric mixtures of Epon and Jeffamine® using a multi-step cross-link algorithm. In MD simulations, atomic interactions are modeled by both General AMBER Force Field (GAFF) and reactive force field ReaxFF to establish the limit of applicability of the GAFF predicting stress-strain responses. Simulation results show that epoxy systems with lower MW cross-linker and higher degree of cure have closely packed, higher density structures. Such structures give higher T_g. With the Williams-Landel-Ferry (WLF) correction considering its universal constants, MD predicted T_g agrees well with the experiments. MD shows linear relationship between T_g and degree of cure and that $\lambda = 1$ should be used in the DiBenedetto relation versus $\lambda = 0.71 - 0.78$ reported in the literature. Epoxy with lower MW cross-linker and higher degree of cure give higher modulus and strength. However, lower MW cross-linker gives low strain to failure and low absorbed energy. Results indicate that energy absorption can be tailored by blending different MW cross-linkers. Stress-strain responses predicted by GAFF agree with ReaxFF at low strain range (up to strain hardening), and then deviate significantly when failure initiates through bond breakage.

Declaration of competing interest

We do not have any conflict of interest.

Acknowledgment

Research was sponsored by the Army Research Laboratory and was accomplished under Cooperative Agreement Number W911NF-12-2-0022. The views and conclusions contained in this document are those of the authors and should not be interpreted as representing the official policies, either expressed or implied, of the Army Research Laboratory or the U.S. Government. The U.S. Government is authorized to reproduce and distribute reprints for Government purposes notwithstanding any copyright notation herein. SCC would like to thanks Chaitanya M. Daksha (UD-CCM intern) for his help in data reduction.

Appendix A. Bond force and energy data

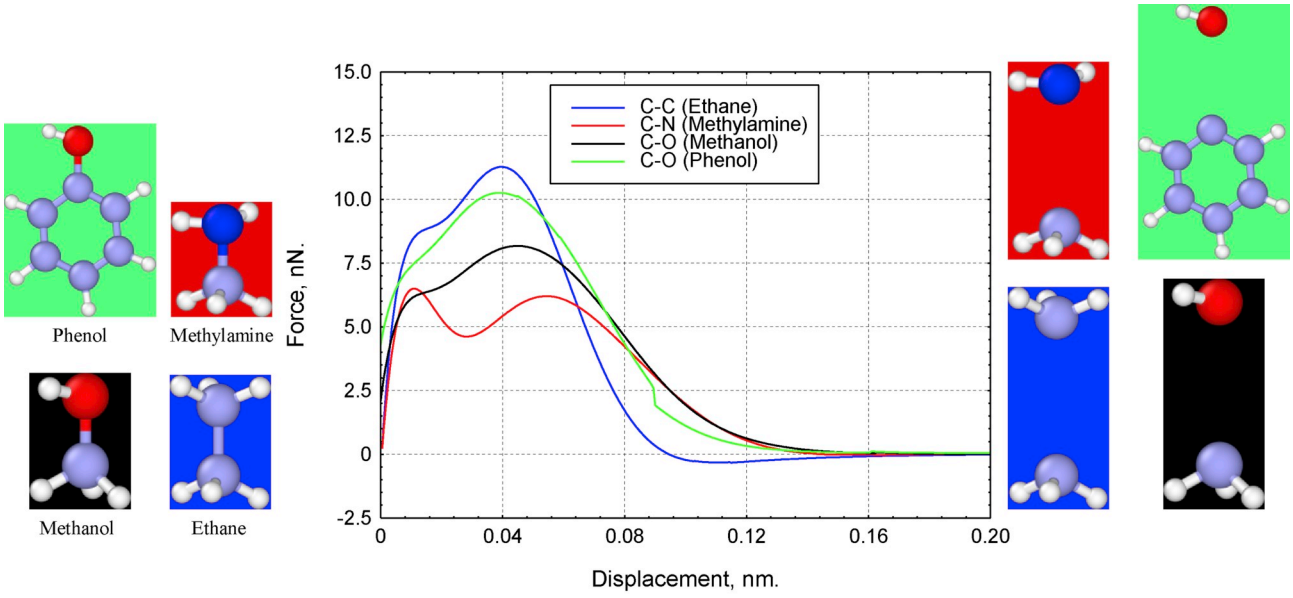

(a) Force-displacement responses. (Molecules without and with broken bond are shown in the left and right sides).

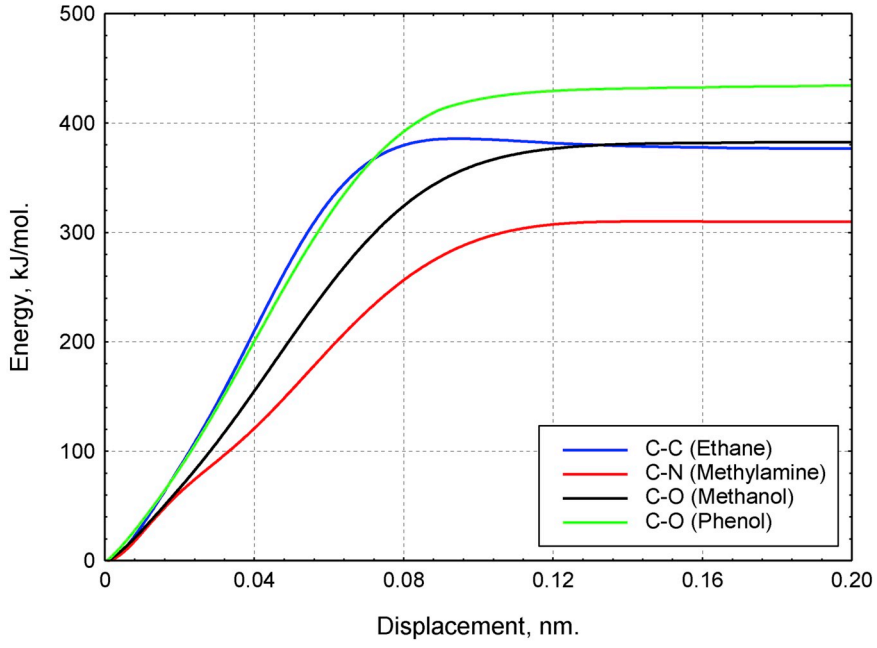

(b) Energy-displacement response.

Fig. A1. (a) Force-displacement and (b) energy-displacement responses of different bonds.

Table A1
Bond force and energy data.

Bond Type	Peak Force, nN	Energy, kJ/mol
C–N (Methylamine)	6.5	311
C–O (Methanol)	8.2	385
C–O (Phenol)	10.3	438
C–C (Ethane)	11.3	376

Appendix B. Epoxy energy data

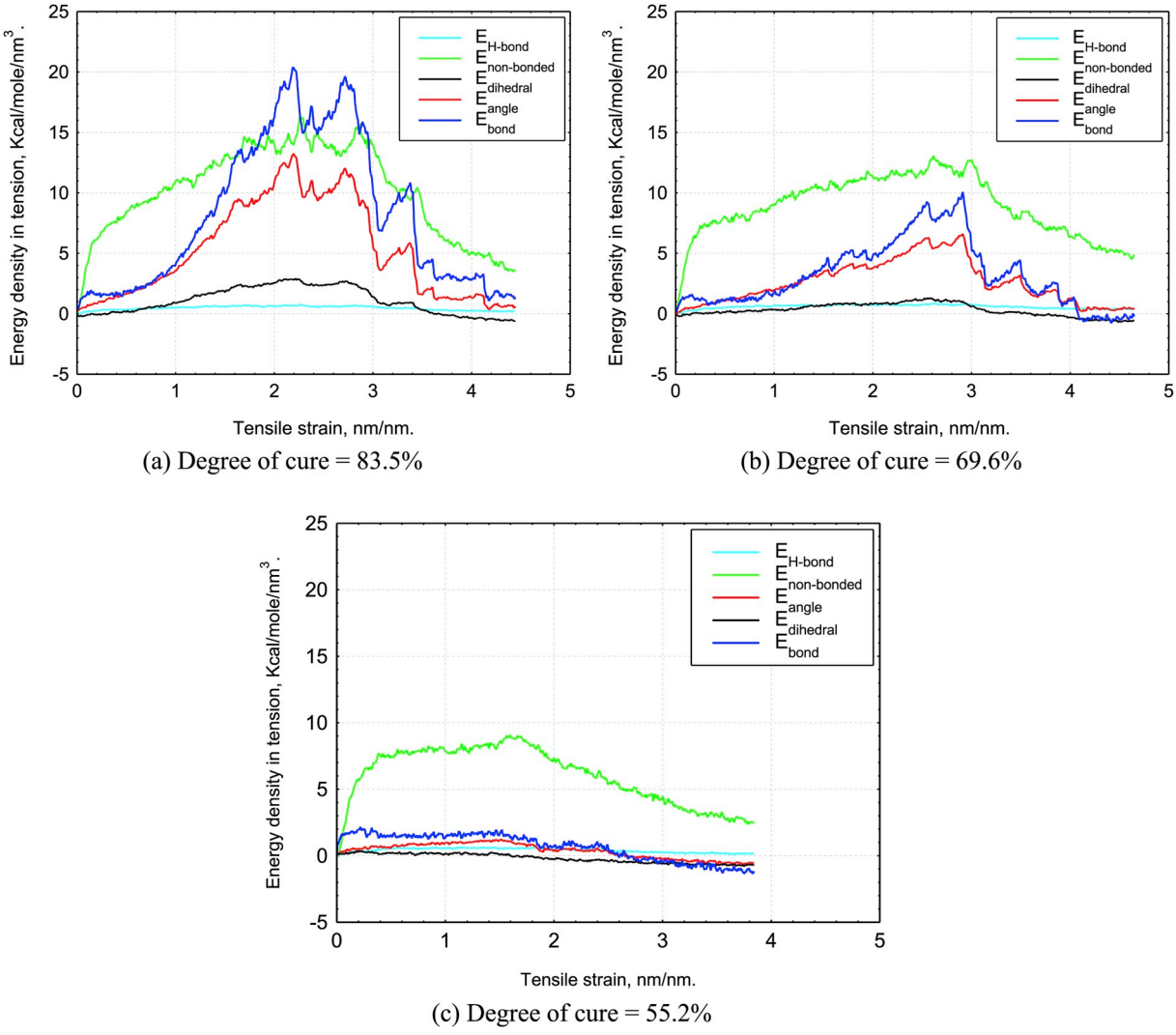

Fig. B1. Variation of energy with tensile strain for different degree of cure for Epon/J230 system.

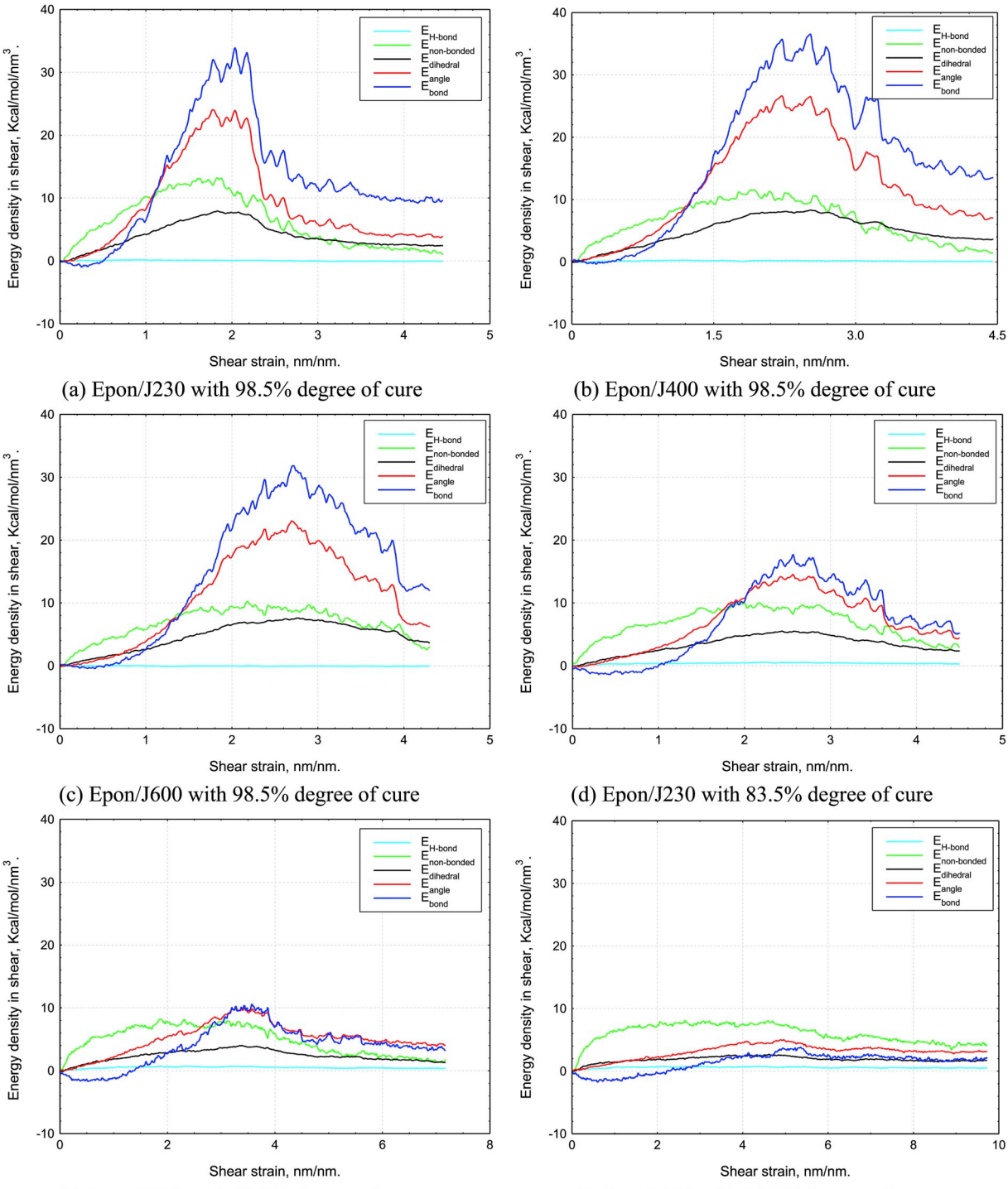

(a) Epon/J230 with 98.5% degree of cure

(b) Epon/J400 with 98.5% degree of cure

(c) Epon/J600 with 98.5% degree of cure

(d) Epon/J230 with 83.5% degree of cure

(e) Epon/J230 with 69.9% degree of cure

(f) Epon/J230 with 55.2% degree of cure

Fig. B2. Variation of energy (ΔE) with shear strain for different MW cross-linker and different degree of cure.

References

[1] Lee A, McKenna GB. Effects of crosslink density on physical ageing of epoxy networks. Polymer 1988;29:1812–7.
[2] Crawford E, Lesser AJ. The effect of network architecture on the thermal and mechanical behavior of epoxy resins. J Polym Sci, Polym Phys Ed 1997;36(8):1371–82.
[3] Vanlandingham MR, Eduljee RF, Gillespie Jr JW. Relationships between stoichiometry, microstructure, and properties for amine-cured epoxies. J Appl Polym Sci 1999;71(5):699–712.
[4] McAninch IM, Palmese GR, Lenhart JL, La Scala JJ. Characterization of epoxies cured with bimodal blends of polyetheramines. J Appl Polym Sci 2013;130(3):1621–31.
[5] Li C, Strachan A. Molecular dynamics predictions of thermal and mechanical properties of thermoset polymer EPON862/DETDA. Polymer 2011;52:2920–8.
[6] Varshney V, Patnaik SS, Roy AK, Farmer BL. A molecular dynamics study of epoxy-based networks: cross-linking procedure and prediction of molecular and material properties. Macromolecules 2008;41:6837–42.
[7] Soni NJ, Lin PH, Khare R. Effect of cross-linker length on the thermal and volumetric properties of cross-linked epoxy networks: a molecular simulation study. Polymer 2012;53(4):1015–9.
[8] Sirk TW, Khare KS, Karim M, Lenhart JL, Andzelm JW, McKenna GB, Khare R. High strain rate mechanical properties of a cross-linked epoxy across the glass transition. Polymer 2013;54(26):7048–57.
[9] Fan HB, Yuen MMF. Material properties of the cross-linked epoxy resin compound predicted by molecular dynamics simulation. Polymer 2007;48:2174–8.
[10] Odegard GM, Jensen BD, Gowtham S, Wu J, He J, Zhang Z. Predicting mechanical response of crosslinked epoxy using ReaxFF. Chem Phys Lett 2014;591:175–8.
[11] Jang C, Sharifi M, Palmese GR, Abrams CF. Crosslink network rearrangement via reactive encapsulation of solvent in epoxy curing: a combined molecular simulation and experimental study. Polymer 2014;55(16):3859–68.
[12] Mayo SL, Olafson BD, Goddard III WA. Dreiding: a generic force field for molecular simulations. J Phys Chem 1990;94:8897–909.
[13] Dauber-Osguthorpe P, Roberts VA, Osguthorpe DJ, Wolff J, Genest M, Hagler AT. Structure and energetics of ligand binding to proteins: Escherichia coli dihydrofolate reductase-trimethoprim, a drug-receptor system. Proteins Struct Funct Genet 1988;4:31–47.
[14] Wang J, Wang W, Kollman PA, Case DA. Automatic atom type and bond type perception in molecular mechanical calculations. J Mol Graph Model 2006;25(2):247–60.
[15] Wang J, Wolf RM, Caldwell JW, Kollman PA, Case DA. Development and testing of a general amber force field. J Comput Chem 2004;25(9):1157–74.
[16] Sun H, Mumby SJ, Maple JR, Hagler AT. An ab initio CFF93 all-atom force field for polycarbonates. J Am Chem Soc 1994;116:2978–87.
[17] Li C, Strachan A. Molecular scale simulations on thermoset polymers: a review. J Polym Sci, Part B: Polym Phys 2015;53:103–22.
[18] Liu L, Liu Y, Zybin SV, Sun H, Goddard WA. ReaxFF-lg: correction of the ReaxFF reactive force field for London dispersion, with applications to the equations of state for energetic materials. J Phys Chem 2011;115:11016–22.
[19] Meng Z, Bessa MA, Xia W, Liu WK, Keten S. Predicting the macroscopic fracture energy of epoxy resins from atomistic molecular simulations. Macromolecules 2016;49:9474–83.
[20] Li C, Jaramillo E, Strachan A. Molecular dynamics simulations on cyclic deformation of an epoxy thermoset. Polymer 2013;54:881–90.
[21] Ganesh R, Sockalingam S, Gillespie Jr JW. Dynamic effects of a single fiber break in unidirectional glass fiber-reinforced polymer composites: effects of matrix plasticity. J Compos Mater 2018;52(14):1873–86.
[22] Senftle TP, et al. The ReaxFF reactive force-field: development, applications and future directions. Npj Comput Mater 2016;2:15011.
[23] Sirk TW, Karim M, Lenhart JL, Andzelm JW, Khare R. Bi-modal polymer networks: viscoelasticity and mechanics from molecular dynamics simulation. Polymer 2016;90:178–86.
[24] Elder RM, Knorr Jr DB, Andzelm JW, Lenhart JL, Sirk TW. Nanovoid formation and mechanics: a comparison of poly(dicyclopentadiene) and epoxy networks from molecular dynamics simulations. Soft Matter 2016;12:4418–34.
[25] Sun H. COMPASS: an ab initio force-field optimized for condensed-phase applications - overview with details on alkane and benzene compounds. J Phys Chem B 1998;102:7338–64.
[26] Jakalian A, Bush BL, Jack DB, Bayly CI. Fast, efficient generation of high-quality atomic charges. AM1-BCC model: I. Method. J Comput Chem 2000;21:132–46.
[27] Jakalian A, Jack DB, Bayly CI. Fast, efficient generation of high-quality atomic charges. AM1-BCC model: II. Parameterization and validation. J Comput Chem 2002;23:1623–41.
[28] Hockney RW, Eastwood JW. Computer simulation using particles. NY: Adam Hilger; 1989.
[29] Rappe AK, Goddard WA. Charge equilibration for molecular dynamics simulations. J Phys Chem;95:3358-3363.
[30] Nakano A. Parallel multilevel preconditioned conjugate-gradient approach to variable-charge molecular dynamics. Comput Phys Commun 1997;104:59–69.
[31] ReaxFF manual. http://www.engr.psu.edu/adri/ReaxffManual.aspx.
[32] https://en.bio-soft.net/3d/ArgusLab.html.
[33] Plimpton S. Fast parallel algorithms for short-range molecular dynamics. J Comput Phys 1995;117(1):1–19.
[34] Jones BH, et al. Stress relaxation in epoxy thermosets via a ferrocene-based amine curing agent. Macromolecules 2017;50:5014–24.
[35] Shinoda W, Shiga M, Mikami M. Rapid estimation of elastic constants by molecular dynamics simulation under constant stress. Phys Rev B 2004;69:134103.
[36] Humphrey W, Dalke A, Schulten K. VMD - visual molecular dynamics. J Mol Graph 1996;14(1):33–8.
[37] Chowdhury SC, Haque BZ(Gama), Gillespie Jr JW. Molecular dynamics simulations of the structure and mechanical properties of silica glass using ReaxFF. J Mater Sci 2016;51:10139–59.
[38] Chowdhury SC, Sockalingam S, Gillespie Jr JW. Molecular dynamics modeling of the effect of axial and transverse compression on the residual tensile properties of ballistic fiber. Fibers 2017;5(7). https://doi.org/10.3390/fib5010007.
[39] Chowdhury SC, Gillespie Jr JW. A molecular dynamics study of the effects of hydrogen bonds on mechanical properties of Kevlar® crystal. Comput Mater Sci 2018;148:286–300.
[40] Clausius R. On a mechanical theorem applicable to heat. Philos Mag A 1870;40:122–7.
[41] Tsai DH. The virial theorem and stress calculation in molecular dynamics. J Chem Phys 1979;70:1375–82.
[42] Thompson AP, Plimpton SJ, Mattson W. General formulation of pressure and stress tensor for arbitrary many-body interaction potentials under periodic boundary conditions. J Chem Phys 2009;131(15):154107.
[43] O'Driscoll ES. Simple and pure shear. Nature 1964;201:672–4.
[44] Maloney CE, Lemaitre A. Amorphous systems in athermal, quasistatic shear. Phys Rev E 2006;74:016118.
[45] Tanguy A, Leonforte F, Barrat J-L. Plastic response of a 2D Lennard-Jones amorphous solid: detailed analysis of the local rearrangements at very slow strain rate. Eur. Phys. J. E 2006;20:355–64.
[46] Monette L, Anderson MP, Wagner HD, Mueller RR. The Young's modulus of silica beads/epoxy composites: experiments and simulations. J Appl Phys 1994;75(3):1442–55.
[47] Wu WL, Bauer BJ. Epoxy network structure. 3. Neutron-scattering study of epoxies containing monomers of different molecular weight. Macromolecules 1986;19(6):1613–8.
[48] Huang MLL, Williams JG. Mechanisms of solidification of epoxy-amine resins during cure. Macromolecules 1994;27(25):7423–8.
[49] Lee A, McKenna GB. Effect of crosslink density on physical ageing of epoxy networks. Polymer 1988;29(10):1812–7.
[50] Williams ML, Landel RF, Ferry JD. The temperature dependence of relaxation mechanisms in amorphous polymers and other glass-forming liquids. J Am Chem Soc 1955;77(14):3701–7.
[51] Khare KS, Phelan Jr FR. Quantitative comparison of atomistic simulations with experiment for a cross-linked epoxy: a specific volume−cooling rate analysis. Macromolecules 2018;51:564–75.
[52] DiBenedetto AT. Prediction of the glass transition temperature of polymers: a model based on the principle of corresponding states. J Polym Sci, Part B: Polym Phys 1987;25:1949–69.
[53] Pascault JP, Williams RJJ. Glass transition temperature versus conversion relationships for thermosetting polymers. J Polym Sci, Part B: Polym Phys 1990;28:85–95.
[54] Tamrakar S, Ganesh R, Sockalingam S, Haque BZ (Gama), Gillespie Jr JW. Experimental investigation of strain rate and temperature dependent response of an epoxy resin undergoing large deformation. Journal of Dynamic Behavior of Materials 2018;4(1):114–28.
[55] Rubinstein M, Colby RH. Polymer physics. New York: Oxford University Press; 2008.
[56] Tamrakar S, Ganesh R, Sockalingham S, Haque BZ, Gillespie Jr JW. Strain rate-dependent large deformation inelastic behavior of epoxy resin. J Compos Mater 2020;54(1):71–87.
[57] Knorr Jr BD, et al. Overcoming the structural versus energy dissipation trade-off in highly crosslinked polymer networks: ultrahigh strain rate response in polydicyclopentadiene. Compos Sci Technol 2015;114:17–25.
[58] Sockalingam S, Dey M, Gillespie Jr JW, Keefe M. Finite element analysis of the microdroplet test method using cohesive zone model of the fiber/matrix interface. Composites Part A 2014;56:239–47.
[59] Moreira DC, Nunes LCS. Comparison of simple and pure shear for an incompressible isotropic hyperelastic material under large deformation. Polym Test 2013;32:240–8.
[60] Rao V, Drzal LT. The dependence of interfacial shear strength on matrix and interphase properties. Polym Compos 1991;12:48–56.